

Serotonin modulates spike probability in the axon initial segment through HCN channels

Kwang Woo Ko^{1,2}, Matthew N Rasband³, Victor Meseguer⁴, Richard H Kramer⁴ & Nace L Golding^{1,2}

The axon initial segment (AIS) serves as the site of action potential initiation in most neurons, but difficulties in isolating the effects of voltage-gated ion channels in the AIS from those of the soma and dendrites have hampered understanding how AIS properties influence neural coding. Here we have combined confocal microscopy, patch-clamp recordings and light-sensitive channel blockers ('photoswitches') in binocular auditory gerbil neurons to show that hyperpolarization and cyclic-nucleotide-gated (HCN) channels are expressed in the AIS and decrease spike probability, in a manner distinct from that of HCN channels in the soma and dendrites. Furthermore, the control of spike threshold by HCN channels in the AIS can be altered through serotonergic modulation of 5-hydroxytryptamine 1A (5-HT_{1A}) receptors, which hyperpolarizes the activation range of HCN channels. As release of serotonin signals changes in motivation and attention states, axonal HCN channels provide a mechanism to translate these signals into changes in the threshold for sensory stimuli.

In most neurons in the brain, excitatory and inhibitory postsynaptic potentials (EPSPs and IPSPs) interact with different types of voltage-gated channels in the dendrites, and the product of these interactions triggers patterns of action potential output in the axon. From classical studies it was hypothesized on the basis of indirect evidence that the site for action potential generation is the axon initial segment¹, later supported with simultaneous somatic and axonal recordings². Within this general framework, however, it is clear that the subtypes and density of voltage-gated ion channels in the AIS vary considerably^{3,4}, contributing to the diversity in spike shapes displayed by different neuron classes⁵. Action potential threshold also depends critically on the length and diameter of the AIS⁶, as well as the spatial pattern of expression of voltage-gated ion channels^{7,8}.

The AIS is plastic: sustained changes in the level of synaptic excitation can trigger changes in both the length of the AIS and its distance from the soma, resulting in compensatory alterations in spike threshold that maintain firing frequency within a neuron's dynamic range^{9,10}. Voltage-gated calcium channels in the AIS have been shown to be important components of the modulatory control of spike initiation. Both T- and R-type voltage-gated calcium channels are expressed in the AIS of several types of neurons, where they may increase the probability of single spikes or contribute to burst firing¹¹. In auditory brainstem neurons, dopamine downregulates T-type channels through a protein kinase C pathway¹². In dentate gyrus granule cells, acetylcholine reduces spike threshold through activation of muscarinic acetylcholine receptors, calcium influx in the AIS via T-type calcium channels and reduction of Kv7 (M-type) potassium currents¹³. Thus, AIS calcium channels and G-protein-coupled receptors provide mechanisms by which the sensitivity of spike generation can be finely tuned.

We have examined action potential initiation in the principal neurons of the medial superior olive (MSO), where control of spike threshold critically influences the processing of cues used for horizontal sound localization¹⁴. Here we show that HCN channels are expressed in the AIS of MSO principal neurons and that the primary role of these axonal channels is to alter action potential threshold, in contrast to the roles of somatic and dendritic channels in shaping the timing and summation of synaptic potentials. We also show that axonal HCN channels and their influence on spike threshold are subject to long-lasting modulation by 5-HT through 5-HT_{1A} receptors. As the activity of the serotonergic system reports changes in motivational state or attention, axonal HCN channels may provide a way for neurons to translate such state changes into adjustments in firing sensitivity.

RESULTS

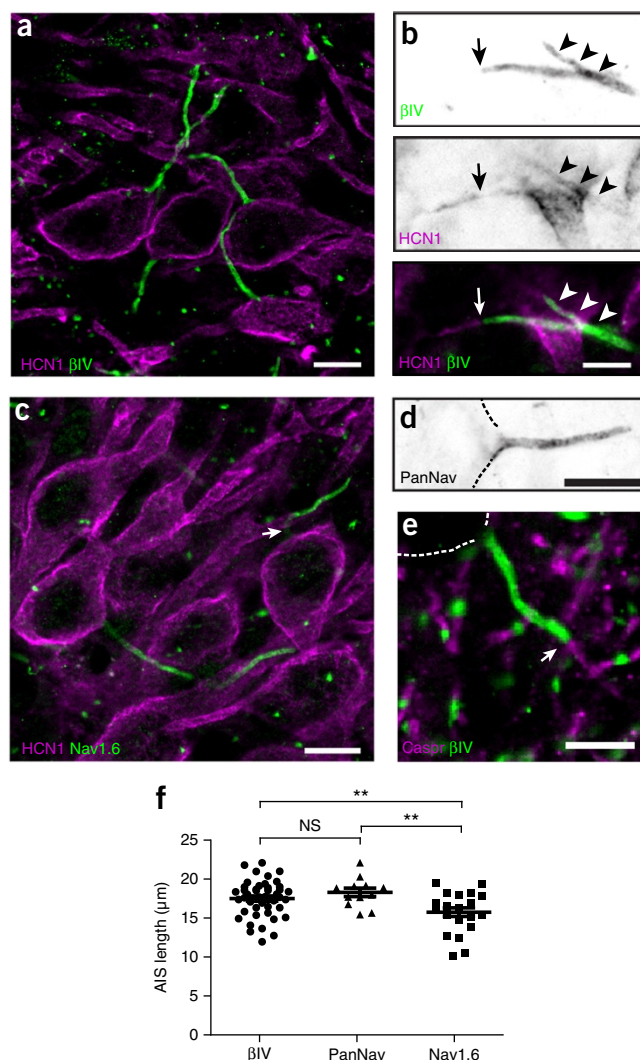
Immunostaining for HCN1 subunits in the AIS

To explore the structural bases underlying action potential initiation and control of threshold in MSO principal neurons, we immunostained sections of gerbil brainstem using antibodies against β IV spectrin, a prominent cytoskeletal scaffold restricted to the AIS and nodes of Ranvier¹⁵, and HCN1 subunits. Although the highest densities of HCN1-containing channels were in the soma and dendrites of MSO neurons (Fig. 1a), we detected low densities of HCN1 channels in 37 of 91 (41%) AIS neurons as well (Fig. 1b). In some instances, HCN1 channels extended beyond the end of the β IV spectrin-labeled AIS (Fig. 1b). In MSO neurons the AIS emanated directly from the soma, rather than a primary dendrite (Fig. 1a). Furthermore, immunostaining for β IV spectrin or pan-specific Nav channel antibody (PanNav, which detects all sodium channel isoforms) began immediately adjacent

¹Department of Neuroscience, University of Texas at Austin, Austin, Texas, USA. ²Center for Learning and Memory, University of Texas at Austin, Austin, Texas, USA. ³Department of Neuroscience, Baylor College of Medicine, Houston, Texas, USA. ⁴Department of Molecular and Cell Biology, University of California, Berkeley, Berkeley, California, USA. Correspondence should be addressed to N.L.G. (golding@austin.utexas.edu).

Received 1 February; accepted 26 March; published online 25 April 2016; doi:10.1038/nn.4293

Figure 1 Expression of HCN1 subunits in the AIS of MSO principal neurons. **(a)** Immunostaining of MSO neurons using antibodies against HCN1 (purple) and β IV spectrin (green). Scale bar, 10 μ m. **(b)** Immunostaining of MSO neuron AIS using antibodies against HCN1 (purple) and β IV spectrin (green). Arrowheads indicate HCN1 immunoreactivity colocalizing with β IV spectrin. The arrow indicates the end of the β IV-spectrin-labeled AIS. HCN1 immunoreactivity frequently extended beyond the end of the AIS into the more distal axon. Scale bar, 5 μ m. **(c)** Immunostaining of MSO neurons using antibodies against HCN1 (purple) and Nav1.6. Nav1.6 immunoreactivity frequently decreased in intensity or was absent immediately adjacent to the cell body (arrow). Scale bar, 10 μ m. **(d)** MSO neuron AIS immunostained using PanNav. This immunoreactivity began at the transition from the cell body to the axon. Dotted lines outline the cell body. Scale bar, 10 μ m. **(e)** Immunostaining of MSO using antibodies against Caspr (purple) and β IV spectrin (green). The arrow indicates the end of the AIS and the start of the myelin sheath. Scale bar, 10 μ m. **(f)** Lengths of β IV spectrin, PanNav and Nav1.6 labeling along the AIS of MSO neurons. Nav1.6 labeling was significantly shorter than either β IV spectrin or PanNav staining, reflecting the reduced staining near the cell body. β IV spectrin, $n = 46$; PanNav, $n = 12$; Nav1.6, $n = 22$. β IV spectrin versus PanNav, $P = 0.2$; β IV spectrin versus Nav1.6, $P = 0.006$; PanNav versus Nav1.6, $P = 0.001$ (unpaired t -test with Welch's correction). Scatterplots show mean \pm s.e.m.; NS, non-significant; ** $P < 0.01$.



to the cell body and averaged $17.4 \pm 0.3 \mu\text{m}$ ($n = 46$ axons from 3 gerbils) and $18.2 \pm 0.5 \mu\text{m}$ ($n = 12$ axons from 3 gerbils) in length, respectively (Fig. 1a,d,f; $P = 0.2$). Intriguingly, immunostaining with antibodies against Nav1.6 Na channels revealed a prominent gap or reduction in immunoreactivity at the proximal end of the AIS, with the highest levels of Nav1.6 at the distal end (Fig. 1c); this distribution of Nav1.6 is reminiscent of that found in cortical pyramidal neurons and retinal ganglion cells^{7,16}. Consistent with this reduction in Nav1.6 immunoreactivity at the proximal AIS, we measured a shorter AIS length when defined by Nav1.6 immunoreactivity (Fig. 1f; $15.6 \pm 0.5 \mu\text{m}$, $n = 22$; $P = 0.0062$ for β IV spectrin length versus Nav1.6 length and $P = 0.0016$ for PanNav length versus Nav1.6 length; unpaired t -test with Welch's correction). In some neurons, the distal end of the AIS also corresponded to the start of myelination, as indicated by immunostaining for the paranodal axoglial junction marker Caspr (Fig. 1e). Together, these results reveal molecular and structural details of the AIS of MSO neurons, including the presence of HCN1 channels.

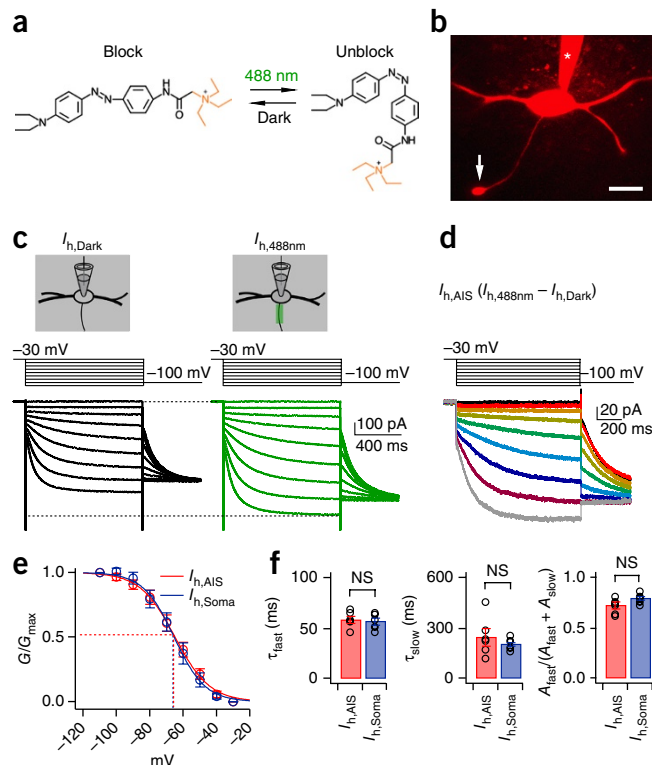
Function of HCN channels in the AIS using photoswitches

To investigate the expression and functional roles of HCN channels in the AIS, we combined confocal microscopy, electrophysiology, and optical manipulation of photoswitches, photoisomerizable compounds that can block the pores of certain voltage-gated ion channels in a wavelength-dependent fashion (Fig. 2a)¹⁷. To directly measure the biophysical properties of HCN channels in the AIS, we made whole-cell voltage-clamp recordings in MSO neurons from gerbils 18–23 d old and isolated the hyperpolarization-activated current (I_h) pharmacologically (Fig. 2b and Online Methods). In these experiments we used DENAQ, which photoswitches to the *cis* (unblocking) configuration with 488-nm light and spontaneously reverts to the *trans* (blocking) configuration in darkness (Supplementary Fig. 1). In the dark DENAQ does not block I_h with 100% efficiency, yielding reduced currents in response to voltage steps (1 s duration) from -30 mV to -110 mV in 10 mV increments (Fig. 2c). When the AIS was scanned with 488 nm light, DENAQ block of voltage-gated channels was relieved and the I_h in the AIS was augmented ($I_{h,488\text{nm}}$; Fig. 2c). Subtraction of the $I_{h,488\text{nm}}$ from $I_{h,\text{Dark}}$ yielded I_h isolated from the AIS ($I_{h,\text{AIS}}$; Fig. 2d). Tail current analysis of $I_{h,\text{AIS}}$ yielded a half-maximal

activation voltage ($V_{1/2}$) of -64.4 ± 2.6 mV, with a slope of 10.0 ± 0.8 ($n = 6$; Fig. 2e). These values were not significantly different from those obtained with somatic block (Fig. 2e; $I_{h,\text{Soma}}$: $V_{1/2} = -65.7 \pm 2.9$ mV, slope = 8.7 ± 0.9 , $V_{1/2}$, $P = 0.74$; slope, $P = 0.27$; $n = 6$). Finally, the activation kinetics of $I_{h,\text{AIS}}$ and $I_{h,\text{Soma}}$ (which exhibited both fast and slow time constants, τ_{fast} and τ_{slow}) were not significantly different from one another, nor was the relative contribution of each of these components as a proportion of the total current amplitude (Fig. 2f). These findings confirm the presence of I_h in the AIS of MSO cells and also show that these channels display many of the same biophysical properties as those found throughout the rest of the cell.

To understand the functional roles of HCN channels in the AIS, we performed experiments using whole-cell current-clamp recordings with AAQ (acrylamide-azobenzene-quaternary ammonium). AAQ was maintained in its *cis* conformation with field illumination at 380 nm, which maintains channels in an unblocked state (Fig. 3a). Local channel blockade was achieved by scanning the AIS, soma or whole cell with the confocal microscope's 488-nm laser line (Fig. 3b). A family of simulated excitatory postsynaptic currents (EPSCs) was injected through the patch pipette (0 to 4,000 pA, 800 pA increments), giving rise to simulated postsynaptic potentials and typically to action potentials in response to stronger stimuli (Fig. 3b). Light-regulated channel blockade of the AIS, soma and whole cell reversibly hyperpolarized the membrane resting potential (Fig. 3b,c). However, changes in resting

Figure 2 Activation properties of axonal I_h , as revealed by laser scanning of the photoswitch DENAQ. (a) The *cis* (unblocking) conformation of DENAQ is maintained at 488 nm light (green) while the *trans* (blocking) conformation is maintained in the dark (black). (b) Confocal image of an MSO principal neuron. Arrow, axon bleb; asterisk, patch pipette; scale bar, 30 μ m. (c) Measurement of I_h in the AIS using DENAQ and whole-cell voltage-clamp recordings. Pharmacologically isolated I_h was partially blocked in the dark (black traces) and then focally unblocked in the AIS at 488 nm (green traces). Voltage steps -30 mV to -110 mV in -10 mV steps, 1 s duration. (d) $I_{h,AIS}$ yielded from subtraction of $I_{h,Dark}$ from $I_{h,488nm}$ ($I_{h,AIS} = I_{h,488nm} - I_{h,Dark}$). Instantaneous tail currents measured at -100 mV (colors are for clarity of visualization). (e) The voltage dependence and slope of I_h in the AIS are not significantly different from those in the soma ($V_{1/2}$, $P = 0.74$; slope, $P = 0.27$; $n = 6$; two-tailed unpaired t test; G/G_{max} , ratio of conductance to maximum conductance). (f) I_h values in the axon and soma exhibit fast and slow exponential components, and each component is statistically indistinguishable between the two locations, as is the relative proportion of their current amplitudes (A_{fast} and A_{slow}) (τ_{fast} , $P = 0.56$; τ_{slow} , $P = 0.33$; $[A_{fast}/(A_{fast} + A_{slow})]$, $P = 0.08$; two-tailed, unpaired t test; NS, not significant). Error bars indicate s.e.m.



potential were blocked completely when ZD7288 (20 μ M), a non-photosensitive blocker of HCN channels, was included in the patch pipette solution (Fig. 3c). AAQ is known to block multiple channel types, raising the possibility that nonspecific actions contribute to light-induced changes in resting potential. Bath application of 10 μ M ZD7288 or 2 mM CsCl hyperpolarized MSO cells by an average of 6–7 mV when we maintained AAQ in the unblocked configuration under 380 nm illumination (Fig. 3c). However, after we restored the resting potential to control values via direct current injected through the pipette, no significant changes in resting potential occurred with

488 nm scanning of either the whole cell or AIS (Fig. 3c). Finally, 5 μ M XE-991, a blocker of K_{v7} (KCNQ) potassium channels that are present in the AIS of some cell types, did not significantly alter

Figure 3 Compartment-specific block of resting conductances by laser scanning of AAQ.

(a) The unblocking and blocking conformations of AAQ are maintained at 380 and 488 nm light, respectively. R, acrylamide group; QA, quaternary ammonium group. (b) Scanning blockade of different cellular compartments reversibly alters the resting potential and duration of responses to simulated EPSCs during whole-cell current-clamp recordings. Purple and green traces: unblocked and blocked conformations of AAQ, respectively. Black traces: simulated EPSCs ($I_{pipette}$), 0–4 nA, 0.8 nA steps. (c) Compartment-specific effects of 488 nm illumination of AAQ on resting potentials (gray bars; $P = 2.8 \times 10^{-4}$ for AIS, $P = 4.72 \times 10^{-7}$ for soma, and $P = 1.3 \times 10^{-4}$ for cell; $n = 9$). The resting potential is not altered by 488-nm scanning in the presence of the HCN channel blocker ZD7288 (20 μ M) applied through the recording pipette (blue bars, ZD7288, “Internal”; $P = 0.07$ for cell, $P = 0.66$ for AIS; $n = 6$). Block of HCN channels with external 10 μ M ZD7288 or 2 mM CsCl hyperpolarizes the resting potential when AAQ is under 380 nm illumination, but after restoration of the membrane potential to control values with DC current, no further changes in voltage are induced with 488 nm scanning (blue bars, ZD7288 “Bath”, $P = 0.012$ for cell at 380 nm, $P = 0.08$ for AIS and $P = 0.86$ for cell at 488 nm, $n = 5$; red bars, Cs⁺ “Bath”, $P = 0.0001$ for cell at 380 nm, $P = 0.24$ for AIS and $P = 0.13$ for cell at 488 nm, $n = 6$). (d) Spatial dependence of photoswitch-induced changes in resting potential. Three ROIs (30 μ m long) were placed adjacently from proximal to distal axonal locations (yellow, blue and green, respectively). Scale bar, 30 μ m. (e) Changes in resting potentials occurred only in the proximal ROI overlapping the AIS (0–30 μ m, $P = 0.0007$; 30–60 μ m, $P = 0.28$; 60–90 μ m, $P = 0.52$; $n = 5$). Paired two-tailed Student’s t -test in c and e. Error bars indicate s.e.m. * $P < 0.05$; *** $P < 0.01$; NS, non-significant.

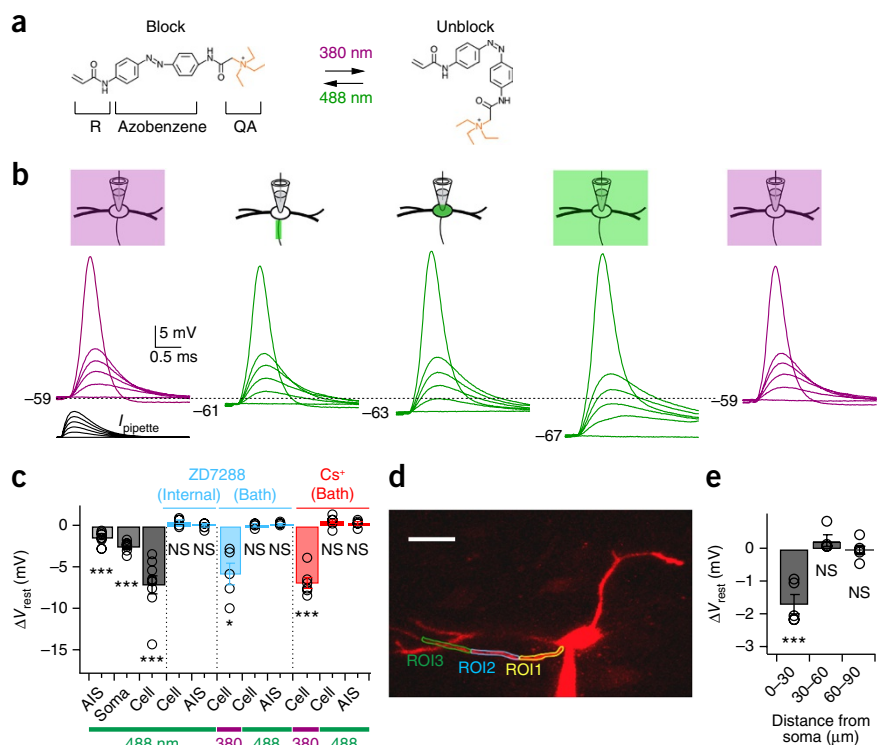
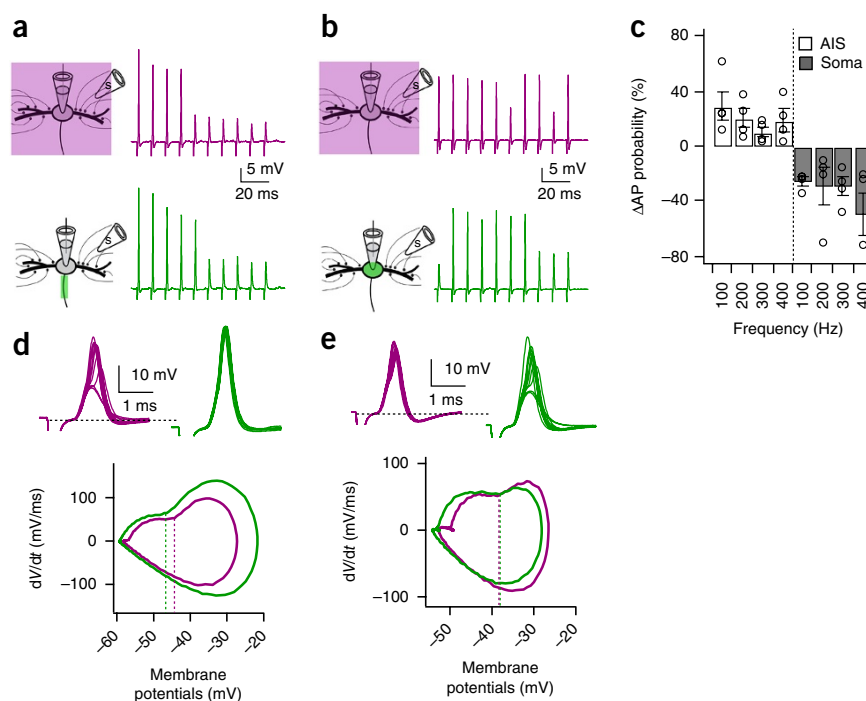


Figure 4 HCN channels in the AIS but not the soma and dendrites decrease spike probability by raising threshold. **(a)** Responses to synaptic stimulation during a whole-cell current-clamp recording with AAQ maintained in the unblocked conformation with 380 nm field illumination (purple traces) and during AIS blockade of HCN channels with focal 488 nm illumination (green traces). Left, experimental configuration; right, responses to contralateral train stimuli (100 Hz, 10 pulses). V_{rest} (380 nm) = -56 mV, V_{rest} (488 nm) = -58 mV. **(b)** In a different cell, identical protocol to that in **a**, except that AAQ-induced blockade was induced in the soma. V_{rest} (380 nm) = -58 mV, V_{rest} (488 nm) = -62 mV. **(c)** Group data showing that the change in spike probability (Δ AP probability) increases during blockade of HCN channels in the AIS (open bars) but decreases during blockade of HCN channels of the soma (gray bars; $n = 4$). Error bars indicate s.e.m. **(d)** Top, the first responses to each of ten stimulus repetitions shown in **a**, superimposed. Bottom, phase plane plot (averaged) of spikes initiated in the traces shown at top. Dashed lines represent the average voltage threshold of spikes in each condition. **(e)** Identical protocol to that in **d**, except data from **b**.



the resting potential (control, -54.1 ± 1.1 mV; XE-991, -55.0 ± 1.0 mV; $P = 0.21$, paired 2-tailed Student's t -test; $n = 6$). Thus the action of AAQ on the resting potential is not explained by its action on other voltage-gated ion channels.

AAQ-mediated changes in the resting potential under 488 nm illumination were restricted to the AIS. In a subset of cells with planar axons over $100 \mu\text{m}$ in length, we scanned 488-nm light in each of three regions of interest (ROIs) drawn over the axon in $30\text{-}\mu\text{m}$ increments (Fig. 3d). Significant light-activated changes in the resting potential were only generated in the proximal compartment encompassing the AIS (Fig. 3e; $0\text{--}30 \mu\text{m}$, $P = 0.0007$; $30\text{--}60 \mu\text{m}$, $P = 0.28$; $60\text{--}90 \mu\text{m}$, $P = 0.52$; $n = 5$), consistent with the expression of HCN1 subunits detected within and just beyond the distal end of the AIS (Fig. 1).

To address the functional influence of HCN channels in the AIS on action potential initiation, we used AAQ to provide focal block of

the AIS or soma during trains of synaptic stimuli delivered to either contralateral or ipsilateral excitatory inputs. In these experiments, GABAergic and glycinergic inhibitory inputs to MSO were blocked by $5 \mu\text{M}$ gabazine and $1 \mu\text{M}$ strychnine. We adjusted the stimulation level to generate approximately a 50% probability of spiking in control conditions (Fig. 4a,b). When HCN channels in the AIS were blocked (Fig. 4a), spike probability increased over a broad range of frequencies (100 Hz: $30 \pm 10.7\%$, 200 Hz: $20 \pm 6.9\%$, 300 Hz: $11 \pm 3.6\%$, 400 Hz: $19 \pm 8.0\%$; $n = 4$; Fig. 4c). By contrast, blocking HCN channels in the soma decreased spike probability (100 Hz: $-26 \pm 3.0\%$, 200 Hz: $-29 \pm 14.6\%$, 300 Hz: $-30 \pm 6.8\%$, 400 Hz: $-49 \pm 15.8\%$; $n = 4$; Fig. 4c). When the shape of action potentials elicited under these conditions was examined with phase plane analysis (Fig. 4d,e), the maximum rate of rise of the action potential (dV/dt) increased by 25% during AIS blockade (86.8 ± 7.5 mV/ms to 109.3 ± 13.5 mV/ms, $P = 0.03$), but only

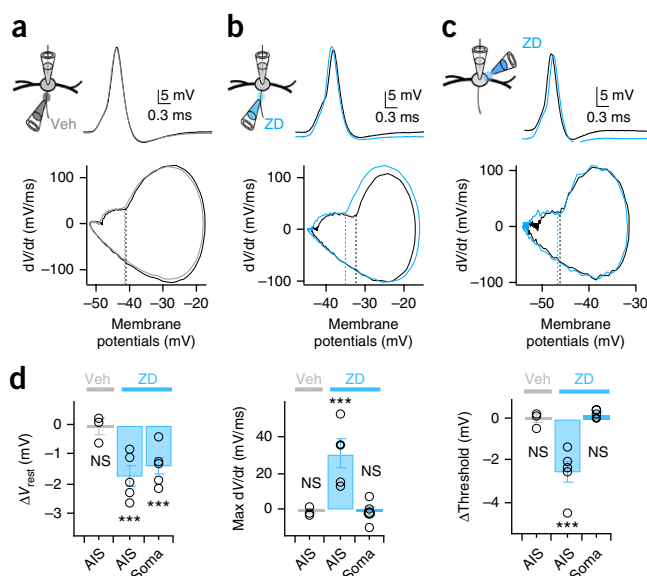
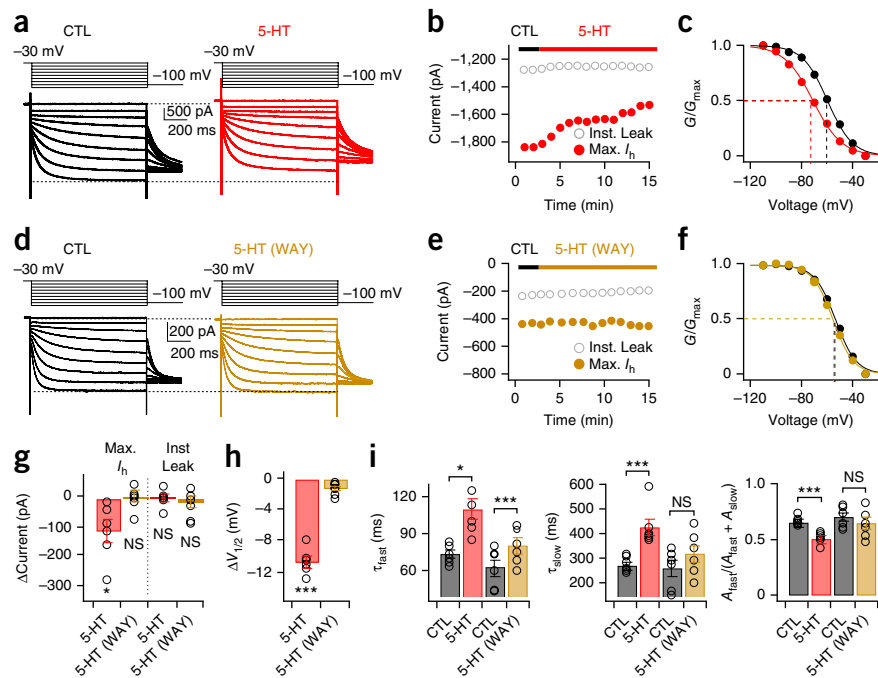


Figure 5 Local pharmacological blockade of HCN channels in the AIS mimics the effects of photoswitches. **(a)** Top, first suprathreshold spike in response to a train of somatic simulated EPSCs (100 Hz; $0\text{--}6$ nA, 0.4 pA steps) in a whole-cell current-clamp recording in control (black) and following brief focal pressure application of a NaCl-based vehicle onto the AIS (gray). Bottom, phase plot of the first spike under each condition. Dotted lines, spike threshold. The vehicle (Veh, gray) altered neither the shape, maximum rate of rise (dV/dt) nor threshold of spikes. $V_{\text{rest}} = -59$ mV for both control and vehicle. **(b)** Brief focal pressure application of $50 \mu\text{M}$ ZD7288 onto the AIS (ZD, blue) hyperpolarized both the resting potential and action potential threshold (phase plot), and increased maximum dV/dt of the spike. $V_{\text{rest}} = -52$ mV (control, Veh), -54 mV (ZD7288). **(c)** Focal application of $50 \mu\text{M}$ ZD7288 to the soma on the opposite side of the AIS hyperpolarized the resting potential but did not change the threshold or shape of the action potential. $V_{\text{rest}} = -59$ mV and -61 mV for control (Veh) and ZD7288, respectively. **(d)** Group data quantifying average ΔV_{rest} , Δ Threshold and Δ Max. dV/dt with focal ZD7288 blockade of HCN channels in the AIS (ΔV_{rest} : Veh, $P = 0.77$, ZD (AIS), $P = 0.07$, ZD (soma), $P = 0.01$; Δ Threshold: Veh, $P = 0.88$, ZD (AIS), $P = 0.008$, ZD (soma), $P = 0.08$; Δ Max. dV/dt : Veh, $P = 0.51$, ZD (AIS), $P = 0.01$, ZD (soma), $P = 0.71$; Veh, $n = 3$; ZD, $n = 5$). Two-tailed paired t test. Error bars indicate s.e.m. *** $P < 0.001$; NS, non-significant.

Figure 6 5-HT modulates the activation range of HCN channels through 5-HT_{1A} receptors.

(a) Voltage dependence of I_h activation in whole-cell voltage-clamp recordings (voltage steps: -30 mV to -110 mV in -10 mV steps, 1 s duration). Black traces, control (CTL); red traces, responses after application of $300 \mu\text{M}$ 5-HT to the soma and axon. (b) Red, maximum I_h (red) during 5-HT application; gray, instantaneous leak current. (c) Plot of normalized conductance shows that $V_{1/2}$ of I_h (dotted lines) shifts negatively after 5-HT application (black, control; red, after 5-HT application; $n = 6$). (d–f) Identical protocol and analyses as in a–c with $10 \mu\text{M}$ WAY100135 (WAY), a 5-HT_{1A} receptor antagonist (brown traces and symbols, $n = 6$). Neither the maximum current nor activation range of I_h is altered in the presence of WAY. (g,h) Group data averaged 11–13 min after 5-HT application for the experiments shown in a–f (5-HT: $\Delta\text{Max. } I_h$, $P = 0.02$; $\Delta\text{Inst. Leak}$, $P = 0.77$; $\Delta V_{1/2}$, $P = 1.8 \times 10^{-5}$; $n = 6$. 5-HT and WAY: $\Delta\text{Max. } I_h$, $P = 0.74$, $\Delta\text{Inst. Leak}$, $P = 0.45$, $\Delta V_{1/2}$, $P = 0.07$; $n = 7$). One-way repeated measures ANOVA. Error bars indicate s.e.m. * $P < 0.05$, *** $P < 0.001$; NS, non-significant. (i) Group data for fast and slow time constants and relative amplitude in the presence of 5-HT and 5-HT with WAY (τ_{fast} : CTL versus 5-HT, $P = 0.01$; CTL versus 5-HT (WAY), $P = 0.0006$; τ_{slow} : CTL versus 5-HT, $P = 0.003$; CTL versus 5-HT (WAY), $P = 0.16$; $A_{\text{fast}}/(A_{\text{fast}} + A_{\text{slow}})$: CTL versus 5-HT, $P = 0.0005$; CTL versus 5-HT (WAY), $P = 0.21$; $n = 6$). Two-tailed paired t test. Error bars indicate s.e.m. * $P < 0.05$, *** $P < 0.001$; NS, non-significant.



9% during somatic blockade (79.8 ± 5.7 mV/ms to 86.9 ± 6.2 mV/ms, $P = 0.06$, paired two-tailed Student's t -test). In addition, the voltage threshold for action potentials was significantly more hyperpolarized during AIS blockade (-1.7 ± 0.4 mV, $P = 0.03$) than for somatic blockade (-0.4 ± 0.3 , $P = 0.24$, paired two-tailed Student's t -test). The effects of somatic photoswitch blockade on spike probability and shape could be offset completely when light-induced changes in resting potential were compensated for by injecting depolarizing current through the recording pipette (Supplementary Fig. 2). In addition, somatic current injection could induce changes in both spike threshold and maximum dV/dt in the soma but required strong hyperpolarization of the membrane potential (≥ 6 mV; Supplementary Fig. 3).

Additional experiments confirmed the involvement of HCN channels in controlling spike probability. In whole-cell current-clamp recordings we generated trains of action potentials at 100 Hz with simulated EPSCs (0 to 6,000 pA in 400 pA increments) and then applied brief puffs of either $50 \mu\text{M}$ ZD7288 or a NaCl-based vehicle focally to the AIS or soma (Fig. 5a–c). In these experiments, we visualized the axon as before with confocal imaging of Alexa-568 and visualized the spread of ZD7288 by monitoring the spread of fast green (1%), included in the puffing solution. The first spike among responses was analyzed for the comparison. When we applied ZD7288 to the AIS, the resting membrane potential of MSO neurons was significantly hyperpolarized (ZD7288: -1.8 ± 0.3 mV, $P = 0.007$; $n = 5$; vehicle: -0.01 ± 0.2 mV, $P = 0.77$; $n = 3$) and the shape of spikes changed (Fig. 5b,d). In addition, phase plane analysis clearly showed that the voltage threshold for action potentials was hyperpolarized (ZD7288: -2.58 ± 0.52 mV, $P = 0.008$; vehicle: -0.04 ± 0.22 mV, $P = 0.88$) and the maximum rate of rise increased (ZD7288: 30.62 ± 7.47 mV/ms, $P = 0.01$; vehicle: -1.25 ± 1.57 mV, $P = 0.51$) during ZD7288 application to the AIS (Fig. 5b,d). Focal application of ZD7288 to the side of the soma opposite the AIS yielded comparable changes in the resting potential (ZD7288: -1.4 ± 0.31 mV, $P = 0.01$; $n = 5$) but did not significantly alter the threshold

(ZD7288: 0.20 ± 0.08 mV, $P = 0.08$) or maximum rate of rise (ZD7288: -1.08 ± 2.73 mV/ms, $P = 0.71$) of the action potential (Fig. 5c,d). The fact that local pharmacological blockade of HCN channels mimics the compartment-specific effects of photoswitches indicates that the effects of AAQ on resting potential, spike threshold and spike shape are due to its blockade of HCN channels.

Modulation of HCN channels by 5-HT

HCN channels are known to be the target of numerous modulatory neurotransmitters. Given the strong influence of HCN channels in the AIS on spike initiation, we asked whether modulation of these channels could influence action potential firing. The MSO receives a dense network of serotonergic fibers arising from the dorsal raphe nucleus^{18,19}. To examine whether 5-HT influences the properties of HCN channels, we made whole-cell voltage-clamp recordings from MSO neurons and isolated I_h pharmacologically (Fig. 6a and Online Methods). When 5-HT ($300 \mu\text{M}$) was continuously applied to the axon, soma and proximal dendrites of MSO neurons via a second patch pipette, the activation range of I_h was significantly shifted in the hyperpolarizing direction (-60.56 ± 1.96 mV to -71.25 ± 2.34 mV, $\Delta V_{1/2} = -10.69 \pm 0.67$ mV, $P = 1.8 \times 10^{-5}$; $n = 6$; Fig. 6a,c,h). While instantaneous leak current was stable in the presence of 5-HT (change in instantaneous leak current ($\Delta\text{Inst. Leak}$) = -3.75 ± 11.93 pA, $P = 0.77$, $n = 6$), the maximum I_h was rapidly and significantly reduced (change in maximum I_h ($\Delta\text{Max. } I_h$) = -119.39 ± 39.37 pA, $P = 0.02$; $n = 6$; Fig. 6b,g). Application of 5-HT also increased both the fast and slow activation time constants of I_h while increasing the relative proportion of total current made up by the slow component (Fig. 6i). The slow component likely reflected the presence of HCN4 subunits in MSO I_h ; blockade of I_h by the heart-slowing drug ivabradine resulted in a slow time-dependent decrease at negative voltages, which has been shown to be a property of channels containing HCN4 but not HCN1 subunits (Supplementary Fig. 4). The modulatory effects of 5-HT on both the

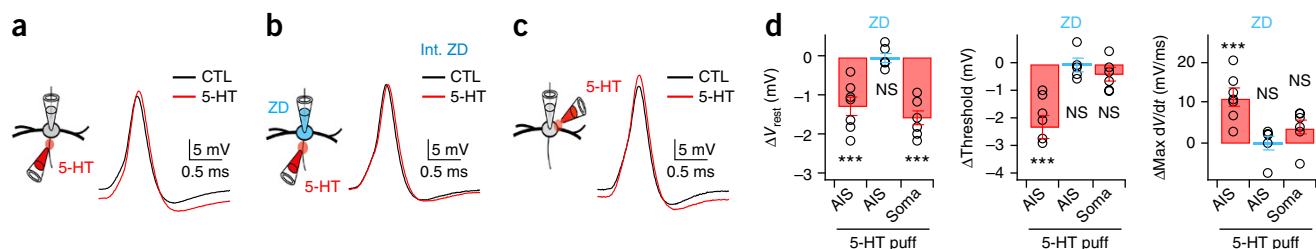


Figure 7 Spike threshold can be controlled by serotonergic modulation of HCN channels in the AIS. **(a)** Focal application of 300 μ M 5-HT onto the AIS (red traces) hyperpolarized the resting membrane potential as well as action potential threshold, as compared to the artificial cerebrospinal fluid (ACSF) control (black traces). $V_{\text{rest}} = -58$ mV and -61 mV for control and 5-HT, respectively. **(b)** The shape and properties of spikes were not altered when 5-HT was applied to the AIS while recording with an intracellular pipette solution containing 20 μ M ZD7288 (Int. ZD). $V_{\text{rest}} = -59$ mV for both control and 5-HT conditions. **(c)** Focal application of 300 μ M 5-HT to the soma on the opposite side of the AIS hyperpolarized the resting potential but did not alter spike threshold or shape. $V_{\text{rest}} = -55$ mV and -57 mV for control and 5-HT, respectively. **(d)** Group data for focal 5-HT application to the AIS in control ACSF (ΔV_{rest} , $P = 0.001$; $\Delta \text{Threshold}$, $P = 0.002$; $\Delta \text{Max. dV/dt}$, $P = 0.002$; $n = 7$), internal ZD7288 (ΔV_{rest} , $P = 0.82$; $\Delta \text{Threshold}$, $P = 0.78$; $\Delta \text{Max. dV/dt}$, $P = 0.92$; $n = 5$), and somatic application (ΔV_{rest} , $P = 0.0004$; $\Delta \text{Threshold}$, $P = 0.10$; $\Delta \text{Max. dV/dt}$, $P = 0.29$; $n = 6$). Paired two-tailed Student's t -test. Error bars indicate s.e.m. *** $P < 0.001$; NS, non-significant.

amplitude and activation voltage of I_h were eliminated in the presence of 10 μ M WAY100135, a 5-HT_{1A} antagonist ($\Delta V_{1/2} = -1.44 \pm 0.29$ mV, $P = 0.07$; $\Delta \text{Max. } I_h = -6.46 \pm 18.68$ pA, $P = 0.74$; $\Delta \text{Inst. Leak} = 27.32 \pm 16.66$ pA, $P = 0.45$; $n = 7$; **Fig. 6d–h**). WAY100135 also strongly attenuated the 5-HT-mediated increase in both activation time constants (though τ_{fast} was still significantly increased versus control), and eliminated significant changes in the relative amplitudes of τ_{fast} and τ_{slow} (**Fig. 6i**). The effects of 5-HT were reversible. In experiments with bath application of 20 μ M 5-HT, the amplitude of I_h was reduced and the $V_{1/2}$ was negatively shifted, as with local 5-HT applications, and these effects reversed within ~ 40 min (**Supplementary Fig. 5**). In addition to 5-HT_{1A} receptors, 5-HT₂ receptors have been reported to negatively shift the activation voltage of HCN channels. However, application of ketanserin (10–50 μ M), a 5-HT₂ antagonist, did not alter 5-HT induced changes in either maximal current amplitude or activation voltages in I_h ($\Delta V_{1/2} = -11.00 \pm 0.28$, $P = 0.013$, $\Delta \text{Max. } I_h = -157.58 \pm 15.68$ pA, $P = 0.002$; $n = 4$).

To understand whether the modulation of HCN channels by 5-HT affects action potential initiation through a local action in the axon, we made whole-cell current-clamp recordings from MSO neurons and focally applied 5-HT (300 μ M) to either the AIS or soma. Application of 5-HT to the AIS hyperpolarized the membrane potential ($\Delta V_{\text{rest}} = -1.29 \pm 0.04$ mV, $P = 0.001$; $n = 7$), decreased spike threshold (change in

voltage threshold, ($\Delta \text{Threshold}$) = -2.29 ± 0.44 mV, $P = 0.002$; $n = 7$) and increased the maximum rate of rise of action potentials ($\Delta \text{Max. dV/dt} = 121.21 \pm 2.20$ mV/ms, $P = 0.002$, $n = 7$) (**Fig. 7a–d**). However, these effects were non-significant when 5-HT was applied to the AIS during recordings in which HCN channels had been blocked by internal application of 20 μ M ZD7288 through the recording pipette (change in resting membrane potential (ΔV_{rest}), -0.03 ± 0.13 mV/ms, $P = 0.82$; $\Delta \text{Threshold}$, -0.08 ± 0.22 mV, $P = 0.78$; change in maximum rate of rise of membrane voltage ($\Delta \text{Max. dV/dt}$), -0.34 ± 3.3 mV/ms, $P = 0.92$; $n = 5$). Finally, focal application of 5-HT to the soma produced changes in the resting potential but no significant changes in spike threshold or maximum dV/dt, similarly to the focal blockade of HCN channels by ZD7288 (**Fig. 7c,d**; ΔV_{rest} , -1.60 ± 0.20 mV, $P = 0.0004$; $\Delta \text{Threshold}$, -0.45 ± 0.23 mV, $P = 0.10$; $\Delta \text{Max. dV/dt}$, 3.60 ± 3.02 mV/ms, $P = 0.29$; $n = 6$).

To address whether 5-HT-induced modulation of spiking can be achieved by physiologically relevant concentrations of 5-HT, we electrically stimulated the plexus of serotonergic axons in and around the MSO during current-clamp recordings while blocking AMPA, NMDA, GABA_A, and glycine receptors with 2,3-dioxo-6-nitro-1,2,3,4-tetrahydrobenzo[f]quinoxaline-7-sulfonamide (NBQX) (10 μ M), AP-5 (50 μ M), gabazine (5 μ M) and strychnine (1 μ M) respectively. We injected simulated EPSCs through the somatic recording pipette every minute for 5 min and monitored both the resting potential and action potentials (**Fig. 8a–d**). Recordings were discontinued if the resting membrane potential was not maintained

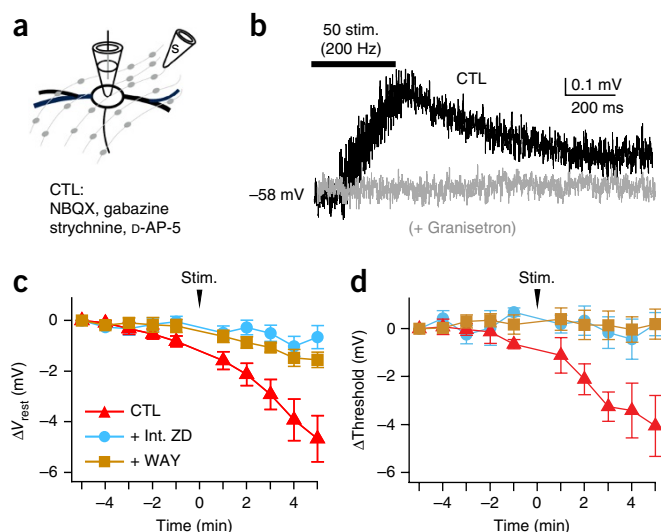


Figure 8 Axonally stimulated release of 5-HT modulates the resting potential and spike threshold of MSO neurons. **(a)** Axonal stimulation (200 Hz, 50 pulses) of serotonergic fibers. Excitatory and inhibitory inputs are blocked (CTL) with 10 μ M NBQX, 50 μ M D(-)-2-amino-5-phosphonopentanoic acid (D-AP-5), 5 μ M gabazine and 1 μ M strychnine. **(b)** Response to a train of contralateral synaptic stimuli (stim.) in ACSF (CTL, black) and 100 μ M granisetron (gray), a blocker of ionotropic 5-HT₃ receptors. **(c,d)** Resting potential and spike threshold were monitored once per minute before and after 200 Hz electrical stimulation (Stim.) of serotonergic axons (50 stimuli). Action potentials were induced via simulated EPSCs injected through the pipette into the soma. At 5 min after stimulation, changes in both resting potential and spike threshold typically induced by 5-HT release (red) could be blocked by 68% and 95%, respectively, in the presence of 0.1 μ M WAY100135 (WAY, brown) or 20 μ M ZD7288 (ZD, blue) dialyzed internally (Int.) through the pipette (CTL: $P = 0.002$ and 0.009 for ΔV_{rest} and $\Delta \text{Threshold}$, $n = 7$; WAY, $P = 0.0039$ and 0.81 for ΔV_{rest} and $\Delta \text{Threshold}$, $n = 8$; ZD: $P = 0.40$ and 0.56 for ΔV_{rest} and $\Delta \text{Threshold}$, $n = 8$). Two-tailed paired t test. Error bars are s.e.m.

within ± 1 mV for 5 min. In these experiments, a train of 50 stimuli at 200 Hz triggered small membrane depolarizations (less than 1 mV) that rose and decayed over hundreds of milliseconds and lacked discrete synaptic events. These slow depolarizations were reduced on average by 85% in the presence of 100 μ M granisetron, an antagonist of ionotropic 5-HT₃ receptors (**Fig. 8b**; control: membrane voltage, 0.53 ± 0.05 mV; granisetron: membrane voltage, 0.06 ± 0.03 mV, $P = 1.9 \times 10^{-5}$; $n = 6$), suggesting that these events represent the paracrine release of 5-HT throughout the slice acting on ionotropic receptors. Correlated with this electrophysiological correlate of stimulated 5-HT release, we observed robust and more long-term hyperpolarization of both the resting membrane potential and spike threshold (**Fig. 8c,d**). Changes in resting potential and spike threshold lasted for the duration of recordings (tens of minutes) and were 68% and 95% blocked, respectively, in the presence of 0.1 μ M WAY100135 (ΔV_{rest} , -1.54 ± 0.31 mV, $P = 0.0039$; $\Delta \text{Threshold}$: 0.19 ± 0.62 mV, $P = 0.81$; $n = 8$) or when recordings were made with 20 μ M internal ZD7288 to block HCN channels (ΔV_{rest} , -0.66 ± 0.45 mV, $P = 0.40$; $\Delta \text{Threshold}$, 0.19 ± 0.49 mV, $P = 0.56$; $n = 8$). Together these results indicate that physiologically released 5-HT is capable of triggering robust changes in the resting potential and action potential threshold of MSO neurons.

DISCUSSION

In most neurons the AIS represents the final stage of synaptic integration, where the complex interplay between excitatory and inhibitory synaptic signals and voltage-gated ion channels determines whether the neuron generates an all-or-none action potential and successfully forwards its signal to its network targets. Action potential initiation sometimes has been regarded as static, exhibiting a discrete and constant threshold. Here we show that HCN channels are expressed in the AIS of auditory neurons in the sound localization circuitry and, by their proximity to the voltage-gated sodium and potassium channels mediating action potentials, regulate spike threshold through their influence on the local resting potential. We further show that modulation of I_h by 5-HT can modify spike threshold through activation of 5-HT_{1A} receptors. Thus HCN channels in the AIS are in a position to adjust spike sensitivity in response to changes in motivation or state of attention.

The AIS of MSO neurons and the expression of HCN subunits

Action potential amplitude is unusually small in MSO principal neurons (5–20 mV), and yet immunolabeling for markers of the AIS show that the AIS is in fact only 12–22 μ m long and emerges directly from the soma with no intervening gap (**Fig. 1**), in strong agreement with previous studies from MSO neurons²⁰ and their avian analogs in low frequency regions of the nucleus laminaris⁶. Immunolabeling of Nav1.6 subunits in MSO neurons was either reduced or absent in the region of the AIS nearest the soma, in results similar to those from retinal ganglion cells and prefrontal cortical neurons^{7,16}. The distal bias of Nav1.6 and the high percentage of inactivated Na channels at the soma²¹ may both contribute to the electrical isolation of the AIS spike generator from the soma and dendrites. The expression of HCN1 subunits both in and slightly distal to the AIS extends previous studies that have shown enrichment of this subunit in the soma and dendrites of MSO neurons^{22–24}. HCN4 (but not HCN2) subunits are also expressed in the soma and dendrites²², but we did not detect the expression of HCN4 subunits in the AIS with antibody labeling (data not shown). Our electrophysiological evidence supports the presence of HCN4 subunits in the axon, however. MSO I_h isolated in the axon or soma exhibited the same dual activation time constants

on time scales of tens and hundreds of milliseconds (**Figs. 2f and 6i**), consistent with the respective kinetics of HCN1 and HCN4 homomeric channels²⁵. MSO I_h exhibits high sensitivity to cAMP, which binds to a cytoplasmic cyclic-nucleotide-binding domain, accelerating channel opening and shifting the activation range to more depolarized voltages²⁶. The activation range of MSO I_h was shifted about -10 mV by modulation of cAMP levels through 5-HT_{1A} receptors, a result more consonant with the presence of HCN4 subunits, which exhibit ~ 2 - to 4-fold higher cAMP sensitivity than HCN1 subunits^{26,27}. A component of MSO I_h recovered from ivabradine blockade at negative voltages, a feature that differentiates HCN4 from HCN1 homomeric channels²⁸. Although we only detected HCN1 subunits in 41% of sampled MSO axons, 100% of photoswitch experiments revealed I_h in the axon. Thus, the complete lack of HCN4 labeling and inconsistent HCN1 labeling in MSO axons probably reflect limits in the sensitivity of the respective antibodies to the relatively low densities of HCN channels in the AIS relative to the soma and dendrites.

Action of photoswitches on HCN channels

MSO neurons express KCNA1 (K_v1) channels at high density. Given that AAQ is known to block several subtypes of voltage-gated potassium channels as a result of its quaternary ammonium group^{17,29}, it is perhaps surprising that the dominant effect of AAQ is predominantly on HCN channels. However, AAQ is an open channel blocker, and given that the average resting potential of MSO neurons sits at the foot of the K_v1 channel activation curve³⁰, the fraction of K_v1 channels active at rest is small relative to that of HCN channels^{22,31}. Accordingly, photoswitching AAQ in 488-nm light had no significant effect on resting membrane potential, spike threshold or spike probability when HCN channels were first blocked pharmacologically (**Figs. 3c and 5 and Supplementary Fig. 6**).

The regulation of spike threshold by HCN channels

HCN channels expressed in the soma and dendrites are critical to synaptic integration: they shape temporal summation^{32–34} and contribute to resonance in firing activity in both cortical and hippocampal neurons during network oscillations^{35,36}. In auditory neurons concerned with preserving submillisecond timing information, including MSO principal neurons, HCN channels provide tonic membrane shunting, which enables fast-rising, precisely timed synaptic events^{22,31,37}. By contrast, in the AIS, we found that HCN channels specifically reduced the probability of action potential firing (**Fig. 4**). Presumably this is mediated in part by an increase in sodium channel inactivation in the AIS, consistent with the increase in the rate of rise of the action potential during AIS-targeted HCN channel blockade. It is also possible that KCNA1 (K_v1) channels, which are enriched in the AIS of both auditory and non-auditory neurons^{8,38}, may also activate through HCN channel activity, decreasing spike probability.

While hyperpolarization of the resting potential occurred with blockade or neuromodulation of HCN channels at both the soma and AIS, spike threshold reduction was far more sensitive to HCN channel manipulations in the AIS (**Supplementary Fig. 3**). Cable properties of the axon versus the soma and dendrites may at least partially account for this disparity. Even modest amplitudes of I_h may produce large local voltage changes in the relatively small-diameter (~ 0.5 μ m) AIS, but the voltage at the soma would be expected to undergo strong attenuation from the unusually large capacitive load imposed by the soma and large caliber dendrites as well as shunting arising from their unusually high resting conductances²². The observations above may also reflect local differences in the density and/or properties of voltage-gated ion channels in the two compartments^{7,11,39}.

Serotonergic modulation of HCN channels in the AIS

Serotonergic projections from the raphe nuclei ramify widely throughout the brain⁴⁰, and they include a dense projection to the MSO and other auditory brainstem nuclei^{18,19}. We found that 5-HT modulates HCN channels in MSO neurons via 5-HT_{1A} receptors, which are coupled to the G proteins (G_i and G_o) that inhibit adenylate cyclase and decrease cAMP concentration⁴¹. Applying 5-HT to whole MSO neurons decreased I_h , hyperpolarized the activation range by ~10 mV and slowed the activation and deactivation kinetics of the channels (Fig. 6), consistent with a decrease in adenylate cyclase activity and reduction in the allosteric modulation of I_h by cAMP^{22,42}. Notably, activation of 5-HT_{1A} receptors by 5-HT, released by stimulation of serotonergic fibers around the MSO, hyperpolarized the resting potential and spike threshold by modulating HCN channels (Fig. 8a–d), reflecting the local action of 5-HT on both the soma and dendrites, as well as the AIS (Fig. 7a–c). In neurons from the spinal cord and prefrontal cortex, the action of 5-HT has been shown to decrease action potential firing through a modulatory decrease in voltage-gated Na⁺ current in the AIS^{43,44}. However, we observed no 5-HT-mediated changes in spike amplitude or shape in our experiments, inconsistent with effects on voltage-gated sodium channels. In MSO neurons, the release of 5-HT, as reported by voltage changes produced by coactivation of ionotropic 5-HT₃ receptors, increased and decayed over hundreds of milliseconds to seconds, consistent with a paracrine release mechanism observed in spinal cord and other auditory brainstem neurons^{43,45}.

Functional implications

The 5-HT-induced decrease in resting HCN channel conductance in the AIS lowers spike threshold without strongly affecting the membrane potential of the soma and dendrites. AIS calcium channels have also been shown to affect both spike probability and pattern, and these influences too can be altered through modulation^{11,12}. These results highlight the critical role of modulatory influences on voltage-gated ion channels in shaping both the probability and pattern of action potentials in the AIS. The functional influence of I_h modulation in the AIS bears some similarity to the effects of blocking AIS-targeted inhibitory inputs in cortical sensory neurons, where response levels increase additively, widening tuning curves without affecting their position^{46,47}. In MSO neurons and their avian analogs, reduction of I_h in the soma and dendrites through modulation or pharmacological blockade has been shown to widen interaural time difference curves *in vitro*^{22,48}. In these studies the reduction in I_h in the soma and dendrites degrades temporal resolution, presumably through an increase in input resistance and membrane time constant. The current findings show that local modulations of spike initiation in the AIS may also influence temporal resolution. Recent studies of synaptic integration in MSO neurons *in vitro* and *in vivo* have underscored the exquisite sensitivity of MSO spike initiation to small changes in resting potential^{49,50}, and thus even subtle modulatory influences on the resting potential and spike probability would have a significant impact on sensory coding.

METHODS

Methods and any associated references are available in the [online version of the paper](#).

Note: Any Supplementary Information and Source Data files are available in the online version of the paper.

ACKNOWLEDGMENTS

The authors would like to acknowledge S. Khurana, who first observed that 5-HT activates 5-HT₃ receptors in MSO neurons. This work was supported by NIH grants NS044916 (M.N.R.), EY024334 (R.H.K.) and DC006877 (N.L.G.).

AUTHOR CONTRIBUTIONS

K.W.K. performed and analyzed all experiments in brain slices. M.N.R. performed and analyzed immunofluorescence labeling experiments. V.M. performed and analyzed experiments in HEK cells. R.H.K. and N.L.G. supervised and helped design experiments in expression systems and slices, respectively. K.W.K. and N.L.G. wrote the main manuscript text with assistance from M.N.R. and R.H.K. M.N.R. prepared Figure 1, K.W.K. prepared Figures 2–8 and Supplementary Figures 2–7, and V.M. and R.H.K. prepared Supplementary Figure 1. All authors reviewed the manuscript.

COMPETING FINANCIAL INTERESTS

The authors declare no competing financial interests.

Reprints and permissions information is available online at <http://www.nature.com/reprints/index.html>.

- Coombs, J.S., Curtis, D.R. & Eccles, J.C. The interpretation of spike potentials of motoneurons. *J. Physiol. (Lond.)* **139**, 198–231 (1957).
- Stuart, G.J. & Sakmann, B. Active propagation of somatic action potentials into neocortical pyramidal cell dendrites. *Nature* **367**, 69–72 (1994).
- Grubb, M.S. *et al.* Short- and long-term plasticity at the axon initial segment. *J. Neurosci.* **31**, 16049–16055 (2011).
- Yoshimura, T. & Rasband, M.N. Axon initial segments: diverse and dynamic neuronal compartments. *Curr. Opin. Neurobiol.* **27**, 96–102 (2014).
- Bean, B.P. The action potential in mammalian central neurons. *Nat. Rev. Neurosci.* **8**, 451–465 (2007).
- Kuba, H., Ishii, T.M. & Ohmori, H. Axonal site of spike initiation enhances auditory coincidence detection. *Nature* **444**, 1069–1072 (2006).
- Hu, W. *et al.* Distinct contributions of Na(v)1.6 and Na(v)1.2 in action potential initiation and backpropagation. *Nat. Neurosci.* **12**, 996–1002 (2009).
- Kole, M.H., Letzkus, J.J. & Stuart, G.J. Axon initial segment Kv1 channels control axonal action potential waveform and synaptic efficacy. *Neuron* **55**, 633–647 (2007).
- Grubb, M.S. & Burrone, J. Activity-dependent relocation of the axon initial segment fine-tunes neuronal excitability. *Nature* **465**, 1070–1074 (2010).
- Kuba, H., Oichi, Y. & Ohmori, H. Presynaptic activity regulates Na(+) channel distribution at the axon initial segment. *Nature* **465**, 1075–1078 (2010).
- Bender, K.J. & Trussell, L.O. Axon initial segment Ca²⁺ channels influence action potential generation and timing. *Neuron* **61**, 259–271 (2009).
- Bender, K.J., Ford, C.P. & Trussell, L.O. Dopaminergic modulation of axon initial segment calcium channels regulates action potential initiation. *Neuron* **68**, 500–511 (2010).
- Martinello, K. *et al.* Cholinergic afferent stimulation induces axonal function plasticity in adult hippocampal granule cells. *Neuron* **85**, 346–363 (2015).
- Grothe, B. New roles for synaptic inhibition in sound localization. *Nat. Rev. Neurosci.* **4**, 540–550 (2003).
- Berghs, S. *et al.* betaIV spectrin, a new spectrin localized at axon initial segments and nodes of ranvier in the central and peripheral nervous system. *J. Cell Biol.* **151**, 985–1002 (2000).
- Van Wart, A., Trimmer, J.S. & Matthews, G. Polarized distribution of ion channels within microdomains of the axon initial segment. *J. Comp. Neurol.* **500**, 339–352 (2007).
- Mourrot, A., Tochitsky, I. & Kramer, R.H. Light at the end of the channel: optical manipulation of intrinsic neuronal excitability with chemical photoswitches. *Front. Mol. Neurosci.* **6**, 5 (2013).
- Hurley, L.M. & Thompson, A.M. Serotonergic innervation of the auditory brainstem of the Mexican free-tailed bat, *Tadarida brasiliensis*. *J. Comp. Neurol.* **435**, 78–88 (2001).
- Thompson, A.M. & Hurley, L.M. Dense serotonergic innervation of principal nuclei of the superior olivary complex in mouse. *Neurosci. Lett.* **356**, 179–182 (2004).
- Lehnert, S. *et al.* Action potential generation in an anatomically constrained model of medial superior olive axons. *J. Neurosci.* **34**, 5370–5384 (2014).
- Scott, L.L., Mathews, P.J. & Golding, N.L. Perisomatic voltage-gated sodium channels actively maintain linear synaptic integration in principal neurons of the medial superior olive. *J. Neurosci.* **30**, 2039–2050 (2010).
- Khurana, S. *et al.* An essential role for modulation of hyperpolarization-activated current in the development of binaural temporal precision. *J. Neurosci.* **32**, 2814–2823 (2012).
- Koch, U., Braun, M., Kapfer, C. & Grothe, B. Distribution of HCN1 and HCN2 in rat auditory brainstem nuclei. *Eur. J. Neurosci.* **20**, 79–91 (2004).
- Kopp-Scheinpflug, C., Pigott, B.M. & Forsythe, I.D. Nitric oxide selectively suppresses IH currents mediated by HCN1-containing channels. *J. Physiol. (Lond.)* **593**, 1685–1700 (2015).
- Santoro, B. *et al.* Molecular and functional heterogeneity of hyperpolarization-activated pacemaker channels in the mouse CNS. *J. Neurosci.* **20**, 5264–5275 (2000).
- Wainger, B.J., DeGennaro, M., Santoro, B., Siegelbaum, S.A. & Tibbs, G.R. Molecular mechanism of cAMP modulation of HCN pacemaker channels. *Nature* **411**, 805–810 (2001).
- Ishii, T.M., Takano, M., Xie, L.-H., Noma, A. & Ohmori, H. Molecular characterization of the hyperpolarization-activated cation channel in rabbit heart sinoatrial node. *J. Biol. Chem.* **274**, 12835–12839 (1999).

28. Bucchi, A., Tognati, A., Milanesi, R., Baruscotti, M. & DiFrancesco, D. Properties of ivabradine-induced block of HCN1 and HCN4 pacemaker channels. *J. Physiol. (Lond.)* **572**, 335–346 (2006).
29. Kramer, R.H., Mouro, A. & Adesnik, H. Optogenetic pharmacology for control of native neuronal signaling proteins. *Nat. Neurosci.* **16**, 816–823 (2013).
30. Mathews, P.J., Jercog, P.E., Rinzel, J., Scott, L.L. & Golding, N.L. Control of submillisecond synaptic timing in binaural coincidence detectors by K(v)1 channels. *Nat. Neurosci.* **13**, 601–609 (2010).
31. Baumann, V.J., Lehnert, S., Leibold, C. & Koch, U. Tonotopic organization of the hyperpolarization-activated current (Ih) in the mammalian medial superior olive. *Front. Neural Circuits* **7**, 117 (2013).
32. Harnett, M.T., Magee, J.C. & Williams, S.R. Distribution and function of HCN channels in the apical dendritic tuft of neocortical pyramidal neurons. *J. Neurosci.* **35**, 1024–1037 (2015).
33. Magee, J.C. Dendritic Ih normalizes temporal summation in hippocampal CA1 neurons. *Nat. Neurosci.* **2**, 848 (1999).
34. Poolos, N.P., Migliore, M. & Johnston, D. Pharmacological upregulation of h-channels reduces the excitability of pyramidal neuron dendrites. *Nat. Neurosci.* **5**, 767–774 (2002).
35. McCormick, D.A. & Pape, H.C. Properties of a hyperpolarization-activated cation current and its role in rhythmic oscillation in thalamic relay neurones. *J. Physiol. (Lond.)* **431**, 291–318 (1990).
36. Narayanan, R. & Johnston, D. Long-term potentiation in rat hippocampal neurons is accompanied by spatially widespread changes in intrinsic oscillatory dynamics and excitability. *Neuron* **56**, 1061–1075 (2007).
37. Golding, N.L., Robertson, D. & Oertel, D. Recordings from slices indicate that octopus cells of the cochlear nucleus detect coincident firing of auditory nerve fibers with temporal precision. *J. Neurosci.* **15**, 3138–3153 (1995).
38. Dodson, P.D., Barker, M.C. & Forsythe, I.D. Two heteromeric Kv1 potassium channels differentially regulate action potential firing. *J. Neurosci.* **22**, 6953–6961 (2002).
39. Colbert, C.M. & Pan, E. Ion channel properties underlying axonal action potential initiation in pyramidal neurons. *Nat. Neurosci.* **5**, 533–538 (2002).
40. Steinbusch, H.W. Distribution of serotonin-immunoreactivity in the central nervous system of the rat-cell bodies and terminals. *Neuroscience* **6**, 557–618 (1981).
41. Polter, A.M. & Li, X. 5-HT1A receptor-regulated signal transduction pathways in brain. *Cell. Signal.* **22**, 1406–1412 (2010).
42. Wang, J., Chen, S., Nolan, M.F. & Siegelbaum, S.A. Activity-dependent regulation of HCN pacemaker channels by cyclic AMP: signaling through dynamic allosteric coupling. *Neuron* **36**, 451–461 (2002).
43. Cotel, F., Exley, R., Cragg, S.J. & Perrier, J.F. Serotonin spillover onto the axon initial segment of motoneurons induces central fatigue by inhibiting action potential initiation. *Proc. Natl. Acad. Sci. USA* **110**, 4774–4779 (2013).
44. Yin, L. *et al.* Selective modulation of axonal sodium channel subtypes by 5-HT1A receptor in cortical pyramidal neuron. *Cereb. Cortex* <http://dx.doi.org/10.1093/cercor/bhv245> (2015).
45. Tang, Z.Q. & Trussell, L.O. Serotonergic regulation of excitability of principal cells of the dorsal cochlear nucleus. *J. Neurosci.* **35**, 4540–4551 (2015).
46. Sturgill, J.F. & Isaacson, J.S. Somatostatin cells regulate sensory response fidelity via subtractive inhibition in olfactory cortex. *Nat. Neurosci.* **18**, 531–535 (2015).
47. Wilson, N.R., Runyan, C.A., Wang, F.L. & Sur, M. Division and subtraction by distinct cortical inhibitory networks in vivo. *Nature* **488**, 343–348 (2012).
48. Yamada, R., Kuba, H., Ishii, T.M. & Ohmori, H. Hyperpolarization-activated cyclic nucleotide-gated cation channels regulate auditory coincidence detection in nucleus laminaris of the chick. *J. Neurosci.* **25**, 8867–8877 (2005).
49. Franken, T.P., Roberts, M.T., Wei, L., Golding, N.L. & Joris, P.X. In vivo coincidence detection in mammalian sound localization generates phase delays. *Nat. Neurosci.* **18**, 444–452 (2015).
50. Roberts, M.T., Seeman, S.C. & Golding, N.L. A mechanistic understanding of the role of feedforward inhibition in the mammalian sound localization circuitry. *Neuron* **78**, 923–935 (2013).

ONLINE METHODS

Animal use. All procedures were conducted in accordance with The University of Texas at Austin Institutional Animal Care and Use Committee, following guidelines of the National Institutes of Health.

Immunostaining. Gerbil brains (21 d postnatal) were acutely dissected and drop-fixed in ice cold 4% paraformaldehyde, pH 7.2, for 1 h. We then transferred the brains to 20% sucrose in 0.1 M phosphate buffer (PB) overnight, and then to 30% sucrose in 0.1 M PB until sectioning. We cut 40 μ m thick coronal sections of brainstem on a cryostat and mounted them on coverslips. Sections were then immunostained as described⁵¹ using mouse antibodies against HCN1 (clone N70/28, NeuroMab), PanNav⁵², or Caspr (clone K65/35, NeuroMab), and rabbit antibodies against β IV spectrin⁵³ or Nav1.6 (ref. 54). AIS lengths were measured using Zeiss Zen software (Zeiss, Thornwood, NY) or Image J (NIH). For AIS lengths, the start and end of the AIS was defined as the point at which the immunoreactivity fell below 10% of the maximum fluorescence intensity along the AIS. Statistics were performed using GraphPad Prism.

Brainstem slice preparation. Mongolian gerbils (*Meriones unguiculatus*) of both sexes were obtained from Charles River Laboratories or bred at the Animal Resource Center of the University of Texas at Austin. Litters were group housed and kept on a 12-h light/dark cycle. Gerbils (P18–P23) were anesthetized with isoflurane, decapitated, and the brain rapidly removed in artificial cerebrospinal fluid (ACSF) at 32 °C. ACSF was bubbled with 95% O₂ and 5% CO₂ and contained 125 mM NaCl, 25 mM glucose, 25 mM NaHCO₃, 2.5 mM KCl, 1.25 mM NaH₂PO₄, 1.5 mM CaCl₂ and 1.5 mM MgSO₄, pH 7.45. Horizontal or coronal sections containing the superior olivary complex were cut at a thickness of 200 μ m with an oscillating tissue slicer (VT1200S; Leica), incubated at 35 °C for at least 30 min, and then held at room temperature until recording. Selected brain slices were biased toward the middle of the dorso-ventral (tonotopic) axis. MSO neurons were identified by their location in the slice, morphology, and distinct electrophysiological characteristics as in previous studies^{30,55}.

Photoswitch experiments. Brainstem slices were pre-incubated at room temperature in the dark for 20–30 min with either 300 μ M AAQ diluted in ACSF for current-clamp recordings or 200 μ M DENAQ in ACSF for voltage-clamp recordings. Thereafter we used photoswitch-free ACSF for recordings. AAQ and DENAQ were custom synthesized⁵⁶ from Jubilant Chemsys, Ltd, Uttar Pradesh, India. Recordings were performed within 1 h of photoswitch incubation to avoid time-dependent changes in the concentration of photoswitches in the membrane. To visualize the axon, soma and dendrites of MSO neurons, 40 μ M Alexa Fluor 568 hydrazide (Invitrogen, Carlsbad, CA) was included in patch pipette solutions, and allowed to dialyze into neurons for at least 5 min after establishing a whole-cell recording. Alexa Fluor 568 was excited using the 543 nm laser line from a 1 mW HeNe laser through the 40 \times objective of a fixed-stage upright confocal microscope (Leica TCS SP5 II). Excitation at 568 nm did not affect the conformation of AAQ or the intrinsic membrane properties of MSO neurons. Scan speed was 400 Hz (pixel dwell time 4.9 μ s), and ROIs generally occupied ~250 and ~600 pixels for the AIS and soma, respectively.

Current-clamp electrophysiology and imaging with AAQ. All current-clamp recordings were performed at 35 °C in ACSF unless otherwise noted. Recordings were made using heat-polished borosilicate patch pipettes (1.65 mm outer diameter; World Precision Instruments, Sarasota, FL), and had resistances of 3–5 M Ω in ACSF. The internal solution in patch pipettes contained 115 mM potassium gluconate, 20 mM KCl, 10 mM sodium phosphocreatine, 10 mM HEPES, 0.5 mM EGTA, 4 mM MgATP and 0.3 mM NaGTP, and the pH was adjusted to 7.3 with KOH. Recordings were made with a Dagan (Minneapolis, MN) BVC-700A amplifier in current-clamp mode. To focally block voltage-gated ion channels in restricted sub-regions of MSO neurons, we combined whole-cell recordings, confocal microscopy, and the use of AAQ in gerbil brainstem slices. After identifying the intact AIS using 568 nm scans under the confocal microscope, the cell was continuously illuminated with 380 nm light through the epifluorescence port of the microscope, which maintains AAQ in the *cis* (non-blocking) conformation. The AIS, soma, or whole cell was then scanned with 488 nm light driving AAQ to the *trans* (blocking) conformation, while simultaneously discontinuing the 380 nm illumination and initiating data acquisition of electrophysiological responses to real or simulated synaptic stimuli. Since all

of the effects of this ‘photoblockade’ were rapidly reversible upon reintroduction of 380 nm light, electrophysiological responses under 380 nm and 488 nm illumination were interleaved to control both for time dependent concentration changes in AAQ in cell membranes and AAQ molecules entering a non-reversible configuration. Data acquisition was controlled by custom macros programmed in Igor Pro (WaveMetrics, Lake Oswego, OR). Code is available upon request.

The effective spatial resolution of photoswitches was assessed with AAQ. Using a 30 μ m ROI over the AIS, we measured how the change in resting potential at 488 nm was affected by moving the ROI perpendicular to the long axis of the axon in 0.5 μ m steps (Supplementary Fig. 7). The change in membrane potential decreased exponentially with a distance constant of 0.37 μ m, close to the theoretical point spread function of 0.31 μ m at 488 nm, demonstrating that the compartment-specific effects of AAQ blockade are minimally affected by light scattering in the slice. Recordings were only included if the series resistance was <20 M Ω . All reported membrane potentials recorded with K-gluconate are corrected for a liquid junction potential of 10 mV.

Voltage-clamp electrophysiology and imaging with DENAQ. All voltage-clamp recordings were made in whole-cell configuration using an Axopatch 200B amplifier (Molecular Devices), filtered at 3 kHz and acquired to computer at 50 kHz via an Instrutech ITC-18 interface (Heka Instruments). Pipette solutions were identical to those in current-clamp recordings. Experiments were conducted at room temperature in ACSF. To reduce the effects of whole-cell dialysis on the activation voltage of HCN channels we used patch-pipettes with open tip resistances of between 4 and 5 M Ω (as in ref. 22) and the time of data collection was limited to 15 min. Series resistance was compensated by at least 95% and pipettes were coated with Sylgard to reduce capacitance. For pharmacologically isolating *I_h*, the following were added to the external ACSF: 1 mM 3,4-diaminopyridine (3,4-DAP), 10 mM TEA-Cl, 0.2 mM 4-aminopyridine, 0.2 mM BaCl₂, 0.001 mM TTX, 0.05 mM NiCl₂, 0.2 mM CoCl₂, 0.01 mM NBQX, 0.05 mM D-AP5, and 0.001 mM strychnine. DENAQ exhibits the *cis* (unblocked) conformation in visible light (450–550 nm) and relaxes rapidly to the *trans* (blocked) conformation in the dark^{17,57}. Thus, in DENAQ experiments cells were maintained in the dark in the blocked state and then *I_h* was unblocked by scanning regions of interest with the 488 nm laser. *I_h* in ROIs was revealed by subtracting *I_h* records in 488 nm illumination from those recorded in the dark. All reported membrane potentials recorded with K-gluconate are corrected for a liquid junction potential of 10 mV.

Synaptic stimulation. We activated synaptic inputs to MSO cells by delivering brief (0.1 ms) electrical pulses to the slice through patch pipettes (tip diameter: 10 μ m). Stimulation electrodes were placed either medial or lateral to the MSO, activating either contralateral or ipsilateral excitatory inputs from the cochlear nucleus, respectively. The probability of action potentials driven by synaptic excitation was not affected by illumination of AAQ in photoswitch experiments when light-induced changes in postsynaptic resting potential were offset with direct current, precluding significant presynaptic effects of AAQ (Supplementary Fig. 2).

Focal application of ZD7288 or 5-HT. The puffing solution contained 10 mM glucose, 125 mM NaCl, 2.5 mM KCl, 3 mM HEPES, and 1% fast green for monitoring the spread of drugs. ZD7288 (50 μ M) or 5-HT (300 μ M) was included in the puffing solution. Initially we visualized the AIS of MSO neurons through a confocal microscope before gently applying either ZD7288 or 5-HT to the AIS.

Data analysis and statistics. All data analyses were performed using custom routines implemented in Igor Pro (WaveMetrics, Lake Oswego, OR). For voltage-clamp recording, MSO neurons were held at –60 mV, and then depolarized to –30 mV for 1 s to deactivate *I_h*. Subsequently, *I_h* was activated with voltage steps from –30 to –110 mV in 10 mV increments and followed by a 1 s step to –100 mV to elicit tail currents. Peak tail currents were averaged from the 10 ms immediately following the capacitive transient and normalized to minimum and maximum tail currents obtained from –110 mV and –30 mV prepulses, respectively. We quantified the activation range of HCN channels by plotting peak tail currents to maximum and minimum *I_h* and fitting this relationship to a Boltzmann equation of the form $f(V) = 1/(1 + \exp[(V_{1/2} - V)/k])$, where V is the membrane voltage, $V_{1/2}$ is the half-maximal activation voltage, and k is the slope factor. Time constants of activation of *I_h* were measured using bi-exponential fits of tail currents in response to voltage steps from –30 mV to –110 mV. In all experiments, values are presented as mean \pm s.e.m., and statistical significance was assessed using a

two-tailed Student's *t* test or a two-way ANOVA for repeated measures at a significance level of 0.05 unless otherwise indicated. Data distribution was assumed to be normal but this was not formally tested. No statistical methods were used to predetermine sample sizes but they were consistent with other publications in the field. Numbers of replications (*n*) are equal to the number of animals used unless indicated otherwise.

A **Supplementary Methods Checklist** is available.

51. Chang, K.J. *et al.* Glial ankyrins facilitate paranodal axoglial junction assembly. *Nat. Neurosci.* **17**, 1673–1681 (2014).
52. Rasband, M.N. *et al.* Dependence of nodal sodium channel clustering on paranodal axoglial contact in the developing CNS. *J. Neurosci.* **19**, 7516–7528 (1999).
53. Yang, Y., Lacas-Gervais, S., Morest, D.K., Solimena, M. & Rasband, M.N. BetaIV spectrins are essential for membrane stability and the molecular organization of nodes of Ranvier. *J. Neurosci.* **24**, 7230–7240 (2004).
54. Schafer, D.P., Custer, A.W., Shrager, P. & Rasband, M.N. Early events in node of Ranvier formation during myelination and remyelination in the PNS. *Neuron Glia Biol.* **2**, 69–79 (2006).
55. Scott, L.L., Mathews, P.J. & Golding, N.L. Posthearing developmental refinement of temporal processing in principal neurons of the medial superior olive. *J. Neurosci.* **25**, 7887–7895 (2005).
56. Banghart, M.R. *et al.* Photochromic blockers of voltage-gated potassium channels. *Angew. Chem. Int. Edn. Engl.* **48**, 9097–9101 (2009).
57. Tochitsky, I. *et al.* Restoring visual function to blind mice with a photoswitch that exploits electrophysiological remodeling of retinal ganglion cells. *Neuron* **81**, 800–813 (2014).